

Optical model plus resonance analysis of $^{12}\text{C} + ^{12}\text{C}$ elastic scattering

R. A. Parker, A. D. Frawley, and L. C. Dennis

Department of Physics, Florida State University, Tallahassee, Florida 32306

(Received 29 April 1985)

Elastic scattering excitation functions for the $^{12}\text{C} + ^{12}\text{C}$ system have been measured at 12 selected center of mass angles between 30.0° and 90.0° over the center of mass energy range 17.5 to 21.5 MeV in 100 keV steps. The elastic scattering excitation function data have been analyzed with an optical model plus multilevel resonance calculation. The extracted spins for the intermediate structure resonances at 18.3 and 19.2 MeV are 12^+ and 12^+ . The structure at 20.2 MeV is due to at least two levels which we have assigned spins of 12^+ and 14^+ .

INTRODUCTION

Elastic scattering measurements for the $^{12}\text{C} + ^{12}\text{C}$ system have been made over a wide range of bombarding energies.¹⁻¹⁰ The usual technique used to extract J^π values for the intermediate structures observed in the elastic channel has been to apply a phase shift analysis to elastic scattering angular distribution data.

The total reaction cross section¹¹ for the $^{12}\text{C} + ^{12}\text{C}$ system exhibits three prominent peaks at $E_{\text{c.m.}} = 18.4$, 19.3, and 20.3 MeV, which correlate well with peaks observed in the 90.0° degree elastic scattering excitation function data.¹² In Fig. 1 our 90.0° degree elastic scattering data are compared to the total reaction cross section data of Ref. 11.

Recently, Ledoux *et al.* have measured extensive angular distribution data at 100 keV intervals for energies between $E_{\text{c.m.}} = 17.8$ and 21.4 MeV.⁷ After applying a phase shift analysis to their elastic scattering angular distribution data Ledoux *et al.* concluded that the resonances at 18.4 and 19.3 MeV were spin 12^+ , while the third resonance at 20.3 MeV was given an ambiguous assignment of 12^+ or 14^+ . To obtain these spin assignments it was necessary that they ignore the elastic scattering data at angles forward of 40.0° , since they could not simultaneously fit the forward and backward angle data.

Using a modified phase shift analysis and the same angular distribution data, Lee *et al.* arrived at spin assignments of 14^+ for the resonances at 19.3 and 20.3 MeV.⁸ The main difference between this analysis and the analysis of Ledoux *et al.* is that Lee *et al.* obtained their nonresonant phase shift parameters from an optical model, using a double-folded real potential.

A phase shift analysis of heavy ion elastic scattering angular distribution data has a number of problems. A major concern is the strength of the resonances. Heavy ion resonances typically have $\Gamma_{\text{el}}/\Gamma < 0.25$, which means that a given resonance does not have as large an effect on the angular distribution as one would like. Another problem is the fact that a large number of parameters (phases and amplitudes for a large number of partial waves) are needed to fit each angular distribution at each energy. Good fits can be obtained with very different sets of parameters,

and therefore some assumptions must be made when choosing between solutions.

The aim of the present work is to investigate the possibility of obtaining more definitive spin assignments for resonances in the $^{12}\text{C} + ^{12}\text{C}$ system from the analysis of elastic scattering excitation function data. Application of the R-matrix theory results in an optical model background plus multilevel resonance (OMMR) description of the elastic scattering excitation function data. The major assumption of this description is that the nonresonant background is described by the optical model. An OMMR analysis has a number of problems of its own. It is difficult to judge whether the background description is adequate; also as the number of resonances of the same spin becomes large, so does the number of parameters needed to describe the data. An attractive feature of excitation function data is that the contribution of certain resonances can be eliminated by measuring the excitation functions at the zeros of the appropriate Legendre polynomials, thereby obtaining simplified subsets of data. Also the effects of a relatively weak resonance in an excitation function are often obvious, where they might be unnoticed

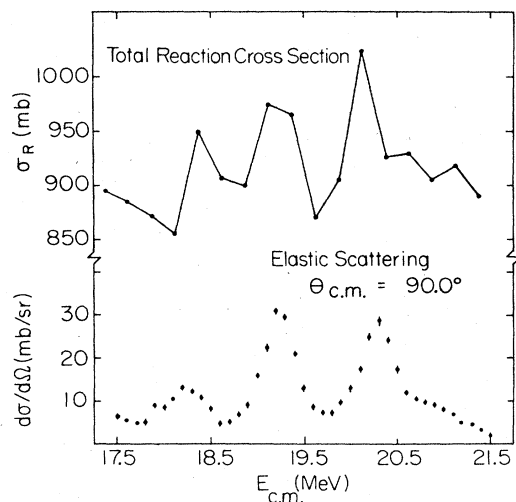


FIG. 1. Total reaction cross section (Ref. 11), together with 90° elastic scattering excitation function data from this study. The curve is to guide the eye.

in angular distribution data.

In this paper we report on the measurements and analysis of elastic scattering excitation function cross sections spanning the energy range $E_{c.m.} = 17.5\text{--}21.5$ MeV for angles between $\theta_{c.m.} = 30.0^\circ$ and 90.0° . The excitation functions were measured at 12 angles, including angles which correspond to zeros of Legendre polynomials, $P_l(\cos\theta) = 0$, for $l = 10, 12, 14, 16$. The analysis of the data with an OMMR code is presented. The region of energy 17.5–21.5 MeV was chosen for this study because of the three large, reasonably well isolated peaks observed in the total reaction cross section (see Fig. 1). This suggested to us that the elastic scattering data in this energy range might be described by a calculation which contained as few as three resonances.

EXPERIMENTAL PROCEDURE

The Florida State University FN tandem accelerator provided ^{12}C beams at energies from $E_{lab} = 35$ to 43 MeV for elastic scattering excitation function and angular distribution measurements on ^{12}C targets. The excitation function data were recorded in 200 keV intervals from 35 to 43 MeV, using natural self-supporting ^{12}C targets having an areal density of $\approx 30 \mu\text{g}/\text{cm}^2$ ($\Delta E_{c.m.} \approx 50$ keV). The angular distribution measurements were recorded using thicker targets of $\approx 150 \mu\text{g}/\text{cm}^2$ ($\Delta E_{c.m.} \approx 300$ keV) at energies of 35 and 43 MeV.

The elastically scattered ^{12}C nuclei were stopped in a surface barrier detector located 22 cm from the target. The absolute detector angle must be known very accurately because the magnitude and energy dependence of the elastic scattering differential cross sections change rapidly with angle, particularly near the zeros of P_l for any of the resonant l values. Placement of the detector was very carefully checked by elastically scattering 20 MeV ^{16}O ions from ^{197}Au targets and comparing the yield at nine angles between $\theta_{c.m.} = 30.0^\circ$ and 110.0° to Rutherford scattering calculations. The angle placement was found to be accurate to ± 0.1 degree.

The 1 mm by 5 mm rectangular detector collimator limited the acceptance angle in the reaction plane to 0.25° for excitation function measurements at angles corresponding to zeros of P_l . The angular acceptance of the detector was limited to 0.5° at all other angles. The collimation of the beam at the entrance to the scattering chamber was provided by two circular collimators 1.6 mm and 0.8 mm in diameter. The smaller collimator was nearest the target and separated from the entrance collimator by 30 cm. Each of the defining collimators was followed by an antiscatter slit. This arrangement gave a beam spot on target of approximately 1 mm diameter. The small beam spot size, combined with the small angular acceptance of the detector, led to a sufficiently small value for the angle averaging in the detector so that the measured energy dependence of the excitation functions was not affected by it, even near the zeros of P_l for resonant values of l .

A fixed-angle monitor with an acceptance angle of 0.9° (laboratory) was placed about 20 cm from the target. The monitor laboratory angle was either 20.0° or 15.0° . The

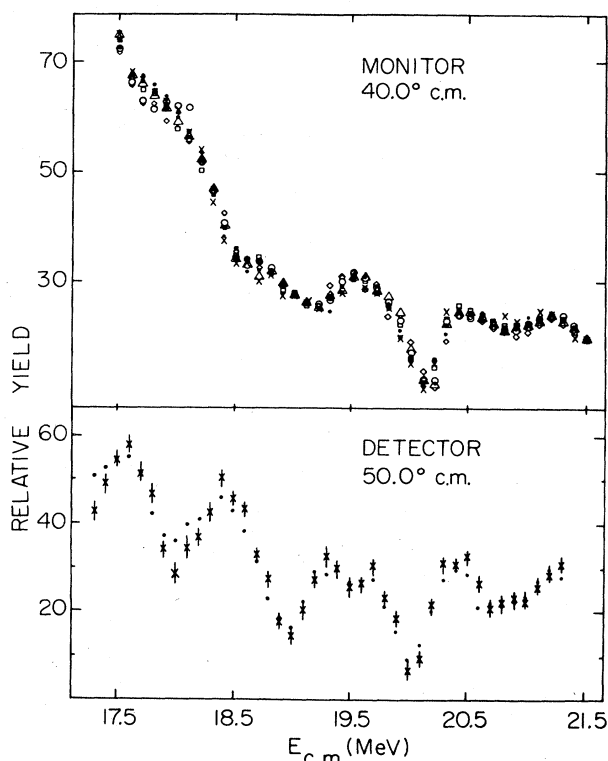


FIG. 2. In the upper panel, monitor excitation function yield curves are compared for seven excitation function measurements. The monitor angle was $\theta_{c.m.} = 40.0^\circ$. The lower panel shows a comparison of two excitation function measurements with the detector at 50.0° .

beam line collimation proved to be adequate for the purpose of minimizing changes in the beam spot position on target, and minimizing changes in the effective beam angle due to focusing. The effectiveness of this arrangement is largely due to the fact that the quadrupole lens nearest to the scattering chamber is located 6 m upstream. In the case where the beam is displaced 1 cm off axis at the quadrupole, the resulting change in beam angle is about 0.1° . The effectiveness of the beam line collimation is demonstrated by the reproducibility of the monitor and detector excitation function yield curves displayed in Fig. 2.

Repeat measurements were performed at widely spaced energy intervals for each excitation function in order to obtain the relative rates of carbon deposition on the targets. The rate of carbon buildup was usually between 1.5 and $3 \mu\text{g}/\text{cm}^2$ over the course of a single excitation function measurement. All data presented in this paper have been corrected for target thickness increase due to carbon deposition on the targets. Angular distribution cross sections were measured at the beam energies $E_{lab} = 35$ and 43 MeV. The angle range of these measurements spanned $\theta_{lab} = 5^\circ$ to 45° in 1° increments. The acceptance angle of the detector was 0.46° , and the accuracy of the angle setting was determined to be $\pm 0.2^\circ$ by comparing the calculated Rutherford scattering cross section to the elastic yield for 20 MeV ^{16}O projectiles scattered from a ^{197}Au target.

The absolute cross section normalizations were obtained by scattering 20 MeV ^{16}O nuclei from the carbon targets and comparing the elastic scattering yield at forward angles to Rutherford scattering calculations. The absolute cross sections are believed to be accurate to $\pm 10\%$.

THEORETICAL CONSIDERATIONS

The differential elastic scattering cross section for spin zero identical particles is given by¹³

$$\frac{d\sigma}{d\Omega} = |f_C(\theta) + f_C(\pi - \theta) + f_n(\theta) + f_n(\pi - \theta)|^2,$$

where $f_C(\theta)$ is the Coulomb scattering amplitude and $f_n(\theta)$ is the nuclear scattering amplitude. The symmetrized nuclear elastic scattering amplitude is expressed as

$$f_n(\theta) + f_n(\pi - \theta) = \frac{2}{k} \sum_{l=\text{even}} (2l+1) \left[\frac{S_l - 1}{2i} \right] \times e^{2i\omega_l} P_l(\cos\theta), \quad (1)$$

where the $P_l(\cos\theta)$ are the Legendre polynomials, the $\omega_l(E)$ are the Coulomb phase shifts, k is the wave number, and the $S_l(E)$ are the elastic scattering matrix elements.

Following the suggestions of Lane and Thomas¹⁴ the scattering matrix $S_l(E)$ is divided into an optical model term which describes the average energy dependence and a second term which describes the resonance. Using the treatment of Robson and Lane^{15,16} the elastic scattering amplitude is written as

$$S_l = S_l^b + ie^{2i(\xi_l + \phi_l^R)} \sum_{\lambda\mu} (\Gamma_{\lambda\lambda, l} \Gamma_{\mu\mu, l})^{1/2} A_{\lambda\mu}. \quad (2)$$

Here S_l^b represents the energy averaged background scattering amplitude. In the formula for the resonant amplitude, ϕ_l^R is the resonance mixing phase, ξ_l is the real part of the background phase shift, and the elastic partial width for a particular level λ is given by $\Gamma_{\lambda\lambda, l}$. The level matrix A is given for the one- and two-level cases by Lane and Thomas.¹⁴ The three-level formula given by Lane and Thomas is incorrect. Using the notation of Lane and Thomas the correct formula is

$$D = \epsilon_1 \epsilon_2 \epsilon_3 - \epsilon_1 \xi_{23}^2 - \epsilon_2 \xi_{13}^2 - \epsilon_3 \xi_{12}^2 - 2\xi_{12} \xi_{13} \xi_{23},$$

$$DA_{11} = \epsilon_2 \epsilon_3 - \xi_{23}^2,$$

$$DA_{22} = \epsilon_1 \epsilon_3 - \xi_{13}^2,$$

$$DA_{33} = \epsilon_1 \epsilon_2 - \xi_{12}^2,$$

$$DA_{12} = DA_{21} = \xi_{12} \epsilon_3 + \xi_{13} \xi_{23},$$

$$DA_{13} = DA_{31} = \xi_{13} \epsilon_2 + \xi_{12} \xi_{23},$$

$$DA_{23} = DA_{32} = \xi_{23} \epsilon_1 + \xi_{12} \xi_{13},$$

where

$$\epsilon_\lambda = E_\lambda - E + \Delta_{\lambda\lambda} - \frac{i}{2} \Gamma_{\lambda\lambda}$$

and

$$\xi_{\lambda\mu} = -\Delta_{\lambda\mu} + \frac{i}{2} \Gamma_{\lambda\mu},$$

E_λ represents the resonance energy for level λ , $\Delta_{\lambda\mu}$ represents the elements of the shift matrix, $\Gamma_{\lambda\mu}$ represents the total widths, and E represents the energy.

To reduce the complexity of this expression the mixing phase and widths Γ are assumed to be independent of energy, and the shift matrix Δ is set to zero.

The background scattering amplitude is given by

$$S_l^b = e^{2i\delta_l},$$

where

$$\delta_l = \xi_l + i\zeta_l.$$

The complex phase shift δ_l is obtained from an optical model. Both ξ_l and ζ_l are real.

The initial values of the background scattering amplitude of Eq. (2) were obtained from optical model fits to the angular distribution data measured at the energies $E_{\text{lab}} = 35$ and 43 MeV ($E_{\text{c.m.}} = 17.5$ and 21.5 MeV). Since the optical potential needed is one which describes the energy averaged behavior of the $^{12}\text{C} + ^{12}\text{C}$ elastic scattering, the angular distribution measurements were performed with thicker targets to provide some averaging over the beam energy. The targets were $\approx 150 \mu\text{g}/\text{cm}^2$ thick, providing $\Delta E_{\text{c.m.}} \approx 300$ keV.

Because it is not known what the correct energy averaged background should be, several different optical potentials were used in conjunction with the resonance analysis. The elastic scattering angular distribution data were fitted with a variety of potential forms, given in Table I.

The best fit which could be obtained with potential form 1 gave an unphysical result for the imaginary diffuseness. The problem was avoided by adding angular-momentum-dependent absorption.¹⁷ However, the only way the data could be fitted simultaneously at 17.5 and 21.5 MeV was to allow for an energy dependence in the depths of the real and imaginary potentials. A linear energy dependence was assumed. Similarly, energy dependences were also needed for potential forms 2, 3, and 4.

The angular distribution data were best described by potential form 5. Phenomenologically, the Woods-Saxon

TABLE I. A list of the background potentials which have been used. The numbers are referred to in the text. WS represents the Wood-Saxon form factor, WS' represents the Wood-Saxon derivative form factor, WS² represents the squared Wood-Saxon form factor, and df represents the double folding potential (Ref. 30).

Potential number	Real potential	Imaginary potential	l dependence
1	WS	WS	no
2	WS	WS'	no
3	WS	WS	yes
4	WS	WS'	yes
5	WS ²	WS	no
6	df	WS	no

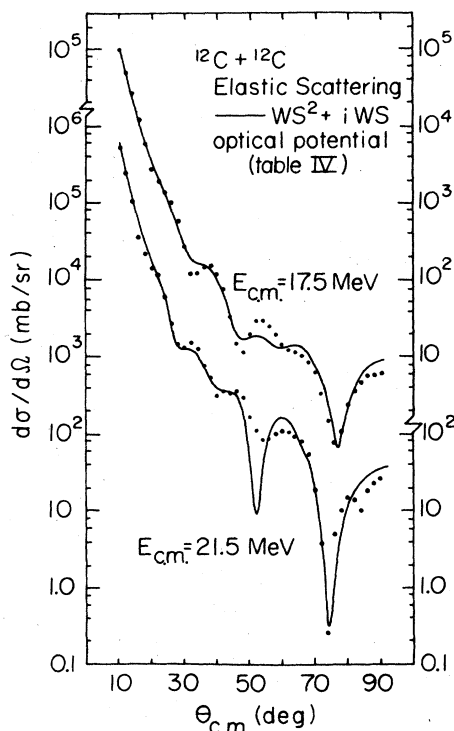


FIG. 3. The elastic scattering angular distribution for $E_{c.m.} = 17.5$ and 21.5 MeV is plotted. The solid curve is from an optical model calculation using potential form 5 (Table IV). The optical potential parameters are obtained from the best fit to the elastic scattering excitation function data.

squared real potential is similar to the real potential obtained from a folding model.^{9,10} Potential 5 was found to require no energy dependence of the potential parameters over the 4 MeV energy span of the calculations. The angular distribution data are plotted in Fig. 3. The solid curve is due to an optical potential of form 5 (Table IV). This potential is the one obtained by fitting the full set of elastic scattering excitation function data with the full OMMR calculation.

In the next section we discuss the analysis of the excitation function data with the OMMR formulation. The computer code written to aid in this analysis allows searching on the background potential parameters as well as the resonance parameters. The parameters for the various optical potentials, obtained by fitting the angular distribution data, were used as starting parameters in the fitting procedure. The calculation time of the OMMR code was reduced significantly by taking advantage of the fact that the optical model phase shifts and amplitudes are at worst quadratically energy dependent over the 4 MeV energy interval of this study. Rather than calculate the optical model S matrix at every energy for an excitation function, the optical model S -matrix elements were calculated at five evenly spaced energies and then interpolated for other energies as needed, reducing the calculation time by an order of magnitude.

RESULTS AND DISCUSSION

In the energy region 17.5 to 21.5 MeV, three large (≈ 100 mb) peaks are observed in the total reaction cross

section.¹¹ The peaks are observed to correlate with peaks in the 90.0° excitation function in the elastic channel.¹² It is tempting to assume that each of these bumps is due to a single resonant state. However, reaction data in this energy range show many resonances, so this assumption is not a safe one. In Table II a compilation^{7,8,18-29} of resonance spins, energies, and widths from previous work for the energy interval 17.5–21.5 MeV is presented. The reported resonances are listed by energy and exit channel in which they were observed. Where more than one reference is given, the resonance was observed in the same channel by different authors. Clearly, some of the structures reported at or near the same energy in different exit channels must be due to the same resonance. Even so, there appear to be about a dozen different resonances reported in this energy range. The complexity of the analysis required in the present work will lie between two extremes. In one extreme, only three of the resonances in Table II might contribute significantly to the total reaction cross section. In the other extreme, many of the resonances in Table II might have a significant effect on the total reaction cross section. In the former case it should be possible to analyze the elastic scattering data with an optical model plus resonance calculation. In the latter case such an analysis will not be tractable.

A natural simplification of the elastic scattering excitation function data occurs when the scattering angle corresponds to a zero of the Legendre polynomial for one of the resonant partial waves. Excitation function data measured at these angles will have no contributions from that partial wave [see Eq. (1)]. In this work, excitation functions have been measured at six angles corresponding to

Table II. Resonances obtained from the literature for the $^{12}\text{C} + ^{12}\text{C}$ system between the energies of 17.5 and 21.5 MeV (c.m.).

$E_{c.m.}$ (MeV)	$\Gamma_{c.m.}$ (keV)	J^π	Exit channel	Reference
17.78	500	12^+	^8Be	23
17.9	340 ± 60		α	29
18.4	400 ± 30		α	29,25
18.4	450	12^+	^{12}C	7
18.4		12^+	^8Be	23
18.5			α	26
18.5			^8Be	28
18.6	375 ± 100		α	29
18.6	300		^8Be	23
18.8	500	12^+	^8Be	23
19.0	310 ± 60	10^+	α	27,29
19.1		12^+	$^{12}\text{C}^*$	20
19.2			α	22
19.3	400	$12^+, 14^+$	^{12}C	7,8
19.3			$^{12}\text{C}^*$	20
19.3	500	12^+	p	18,19,21
19.3			d	21
19.3			n	24
19.4	300 ± 30		α	29
19.6	230	12^+	^8Be	23
19.8		14^+	^{12}C	8
20.4	400,300	$12^+, 14^+$	^{12}C	7,8

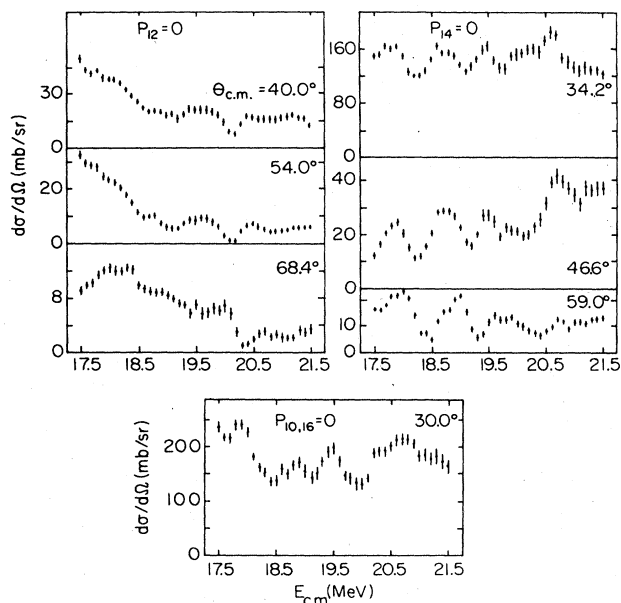


FIG. 4. The $^{12}\text{C} + ^{12}\text{C}$ elastic scattering excitation functions are displayed for angles corresponding to zeros of $P_l(\cos\theta)$, with $l=10,12,14,16$.

the zeros of P_{12} and P_{14} , since the reported resonances are predominantly spin 12 and 14. An excitation function was also measured at a single angle which corresponds to a zero of both P_{10} and P_{16} . These data are shown in Fig. 4.

The excitation function data displayed in Fig. 4 for the angles $\theta_{c.m.}=40^\circ$, 54.0° , and 68.4° are measured at zeros of P_{12} . The data show rather smooth behavior near 18.3 and 19.3 MeV, yet at 20.3 MeV a strong anomaly is still present. Since the excitation function data at all other angles exhibit strong resonant behavior near the energies of 18.3 and 19.3 MeV, it is appropriate to start by assuming that there are 12^+ resonances near 18.3 and 19.3 MeV, just as Ledoux *et al.*¹⁷ reported.

Structure is observed near 20.3 MeV for angles which correspond to zeros of P_{12}, P_{14} and the zero of $P_{10,16}$. Because structure appears at these angles, and in fact at all measured angles, it appears that there are at least two resonances with different spins near 20.3 MeV. A less likely alternative is that the structure at 20.3 MeV is due to a single level with $l \leq 8$ or $l > 16$. This latter alternative was eliminated by comparing the data near 20.3 MeV with calculations assuming single resonances of very low or very high spin.

ANALYSIS OF DATA AT THE ZEROS OF P_{12}

In an effort to obtain the spins of the resonances contributing to the anomaly at 20.3 MeV, an optical model plus single level analysis was performed on the data measured at the zeros of P_{12} . Using potential form 5 as the background, several different mixing phases were chosen for the initial set of resonance parameters and spins between $l=6$ and 18 were tried. The only acceptable fits to these

three excitation functions were obtained for resonances having $l=10$ or 14 with a resonance energy of 20.2 MeV. The fits were almost identical for these two spins. It happens that the value of $(2l+1)|P_l(\cos\theta)|$ is approximately the same (within 15%) for $l=10$ and 14 at the angles 40.0° , 54.0° , and 68.4° . When all of the data are considered, the $l=10$ assignment is eliminated because the calculation gives poor fits at most other angles. In particular, the calculation for $\theta_{c.m.}=90.0^\circ$ gives a dip, when $l=10$ is assumed, where the data clearly indicate a peak. With a 14^+ resonance assumed, the best fit obtained to the data at the zeros of P_{12} is shown as a solid line in Fig. 5. The calculation reproduces the structure at 20.2 MeV for the angles $\theta_{c.m.}=40.0^\circ$ and 68.4° , but the calculated shape for the angle $\theta_{c.m.}=54.0^\circ$ does not reproduce the data as well. To check if this problem is due to angle averaging of the elastic scattering excitation function data (because of the finite size of the detector collimator and beam spot), the calculated differential elastic scattering cross section was integrated over the experimental angle spread ($\Delta\theta_{c.m.}=0.9^\circ$). Assuming unit weighted contributions from all angles inside the limits of the experimental angle spread resulted in negligible changes in the calculated excitation function.

Another candidate for the cause of the discrepancy between the calculation and the data at $\theta_{c.m.}=54.0^\circ$ is the optical model description of the energy averaged background. For the calculations which have been discussed so far, the background was described by potential form 5

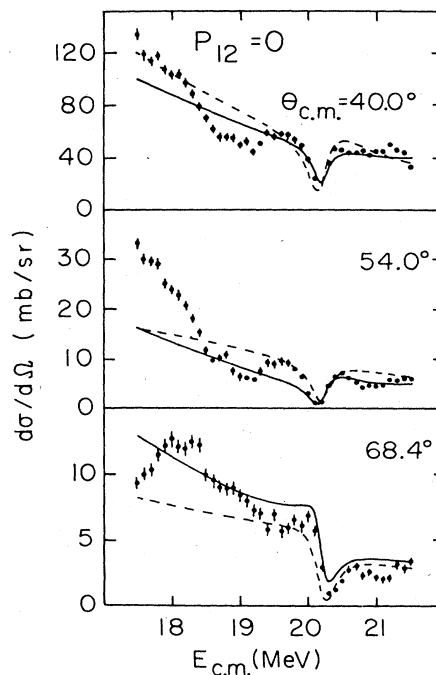


FIG. 5. Elastic scattering excitation functions for three zeros of P_{12} are displayed. The solid curve is an optical model plus single-level resonance calculation using a $WS^2 + i(W)$ optical model background (potential 5 of Table I). The dashed curve is the result of the calculation using a double-folding background (potential 6 of Table I). The single level was located at 20.2 MeV with $l=14$.

because this potential best fit the angular distribution data at 17.5 and 21.5 MeV, and also because the potential parameters were found to be energy independent over the 4 MeV energy interval of the excitation function data. To see if the choice of background potential form makes a difference in the calculation, several other optical model potentials were used in the fitting of the data at the zeros of P_{12} .

Using potential form 6, which has a double-folding real potential, data measured at the zeros of P_{12} were fitted with the optical model plus a single level. The starting resonance parameters for this analysis were obtained from the earlier calculation using potential 5. The fit to the data at the zeros of P_{12} with the double-folding background potential is displayed as a dashed line in Fig. 5. The calculations with potential forms 5 and 6 are similar. The only significant difference between the calculations is in the shape of the resonance around 20.2 MeV for $\theta_{c.m.} = 54.0^\circ$. The folding potential results in a fit which better describes the behavior of the data at the resonance. It appears that some differences in the calculated resonance shapes can be caused by differences in the background description.

ANALYSIS OF DATA AT THE ZEROS OF P_{14}

The data at the zeros of P_{14} were analyzed with an optical model plus three-level formula, using potential form 5. Resonances with $l=12$ were assumed to exist near 18.3, 19.3, and 20.3 MeV. The $l=12$ assignments for the resonances at 18.3 and 19.3 MeV follow from the earlier discussion of the data measured at zeros of P_{12} . The structure near 20.3 MeV was assumed to have spin 12^+ because this structure behaves much like the resonances at 18.3 and 19.3 MeV for the three zeros of P_{14} . These assumptions were tested by trying other spin assignments for the resonances. The initial values of the total widths were obtained from peak width estimates from the total reaction cross section data. Initially, calculations were done with the interference widths set to zero, effectively reducing the three level formula to the sum of three single-level formulae, with all resonances having the same mixing phase. Once the fit converged, all of the resonance parameters were allowed to vary. The best fit to this subset of data is displayed as a solid line in Fig. 6. The data are described rather well around the resonance energies of 18.3 and 19.3 MeV, but the calculation fails at the higher energies. Assuming the structure near 20.3 MeV to have spin 10^+ or 16^+ gave poorer fits to this subset of data and led to severe inconsistencies between the calculation and data at other angles.

The resonant mixing phase for the three-level formula was allowed to vary linearly with energy. The best fit obtained with the variable mixing phase was not better than the previous calculation with a constant mixing phase.

Checking the effects of changing the background description, the data at the zeros of P_{14} were fitted again using potential form 6 and three 12^+ resonances. The results, shown as a dashed line in Fig. 6, were encouraging because the shape and sense of this calculation reproduced

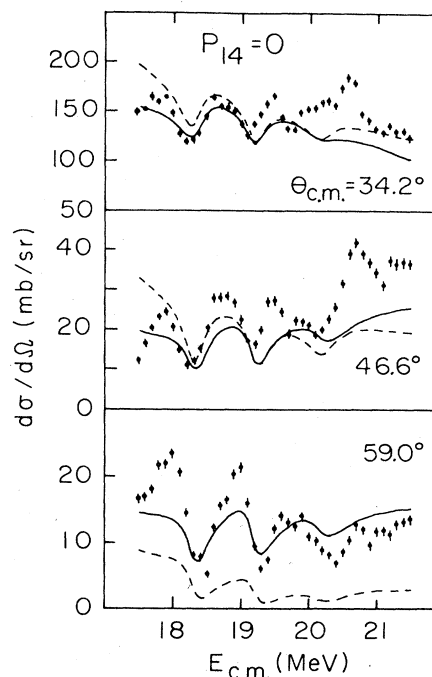


FIG. 6. Elastic scattering excitation functions measured at angles corresponding to zeros of P_{14} . The curves are from optical model plus resonance calculations assuming three $l=12^+$ resonances at 18.3, 19.2, and 20.2 MeV. The solid curve was obtained with potential 5 of Table I as background, the dashed curve with potential 6 of Table I.

the earlier calculations with potential form 5 as the background. However, the folding potential calculation did not reproduce the average magnitude of the data at all three angles. For $\theta_{c.m.} = 59.0^\circ$ the folding calculation gave an average cross section which was about a factor of 3 smaller than the data.

ANALYSIS OF THE FULL DATA SET

Having concluded the analysis of these special subsets of the data, we went to an analysis of the full data set with the OMMR code. Again potential form 5 was used and the initial parameters for the resonances were obtained from the previous analyses of the data at the zeros of P_{12} and P_{14} . The best fit is displayed in Fig. 7; the corresponding level parameters and background potential are summarized in Tables III and IV. As was the case in the analysis of the data at the zeros of P_{14} , the calculation appears to describe the resonances near 18.3 and 19.3 MeV reasonably well; however, there is a marked discrepancy between the calculation and the data at the extreme low energies and high energies. This effect is particularly noticeable at the forward angles. If the forward angle data ($\theta_{c.m.} < 50.0$ degrees) is excluded from the analysis, then an optical model plus resonance calculation which includes three $l=12$ levels and one $l=14$ level is adequate to describe the remaining data. Changing the background potential from potential form 5 to form 6 did not improve the situation. Qualitatively the fit was similar to that obtained with potential form 5, however, at

TABLE III. Resonance parameters used in the calculation displayed in Fig. 7.

λ	E_λ (MeV)	$\Gamma_{\lambda\lambda,l}$ (keV)	$\Gamma_{\lambda\lambda}$ (keV)	ϕ_l^R	Γ_{12} (keV)	Γ_{13} (keV)	Γ_{23} (keV)
Parameters for $l=12$ resonances							
1	18.3	14	336	-157°	629	-295	-238
2	19.2	41	319	-157°			
3	20.2	21	423	-157°			
Parameters for $l=14$ resonance							
1	20.2	30	250	-74°			

some angles the magnitude of the data was underpredicted. The use of potentials 1–4 (Table I) also gave fits to the data which were similar to the calculation using potential 5. However, since these potential forms did a much poorer job of describing the angular distribution data it is not surprising that they severely overpredicted or underpredicted the excitation function data at a few angles. In all cases the spin assignments deduced earlier were supported.

We conclude that more than four resonances are needed to describe the elastic scattering data. Weak single resonances with spins of 10^+ , 12^+ , 14^+ , or 16^+ were placed at selected energies (using Table II as a guide) near the lower and upper energy regions of the excitation function. Minor improvements to the fits were possible, but no dramatic improvement was achieved.

THE FORMAL PARAMETERS

The level parameters quoted by Ledoux *et al.* for the resonances which they reported at 18.4, 19.3, and 20.3 MeV are based on single-level (Breit-Wigner) fits to the extracted phase shifts. The 12^+ parameters given in Table III are formal parameters obtained from a three-level R matrix formulation of the resonant elastic scattering. The use of the three-level formula is necessary because the three $l=12$ resonances overlap significantly. The connection between these formal widths and the widths which one would obtain if this were a single-level problem is difficult to ascertain. Therefore, for the 12^+ resonances, a comparison to the widths given by Ledoux *et al.* is difficult. One could transform the level matrix A into a diagonal form resembling the sum of single levels by using a complex orthogonal transformation matrix, but the newly transformed widths would be complex functions, and also could be strongly energy dependent.¹⁴

A simpler connection between the formal parameters of this work and the level parameters of Ledoux *et al.* can be obtained by comparing plots of the energy dependence of the S matrix in the complex plane. As a function of energy the nonresonant S matrix for a particular l value describes a smooth curve in the complex plane. The addition of a single level resonance formula to the background S matrix

$$S_l = S_l^b + ie^{2i(\phi_l^r + \xi_l)} \frac{\Gamma_{el}}{E_r - E - \frac{i\Gamma}{2}}$$

TABLE IV. Optical potential (potential 5 of Table I) used in the calculation displayed in Fig. 7.

V_0 (MeV)	R_r (fm)	a_r (fm)	W_0 (MeV)	R_i (fm)	a_i (fm)
301	3.36	1.52	2.80	7.09	0.25

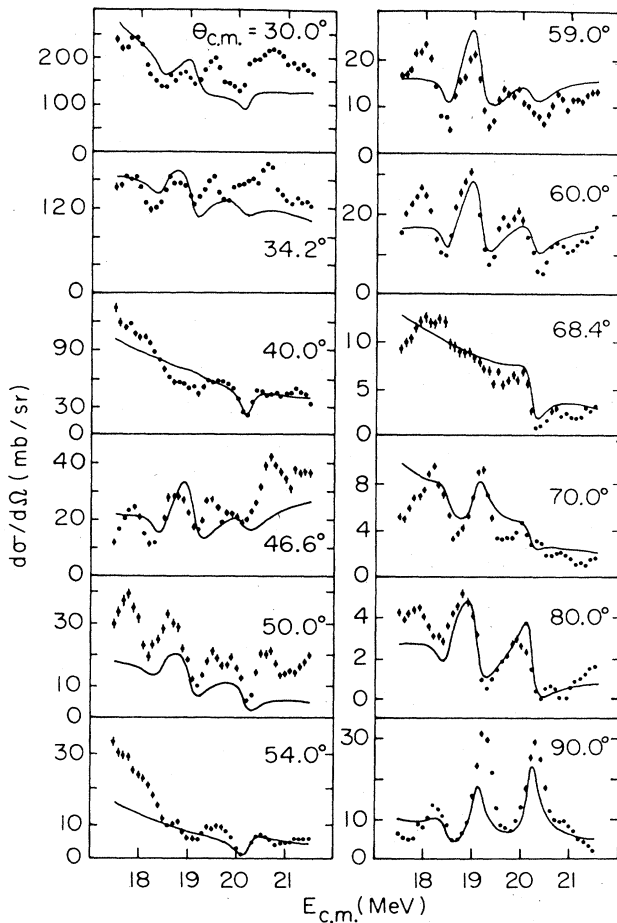


FIG. 7. Elastic scattering excitation function data for the 12 angles measured in this experiment. Curves are from an optical model plus resonance calculation using three $l=12$ resonances located at 18.3, 19.2, and 20.2 MeV, and a resonance with $l=14$ located at 20.2 MeV. The background potential had a $WS^2 + i(WS)$ form (potential 5 of Table I).

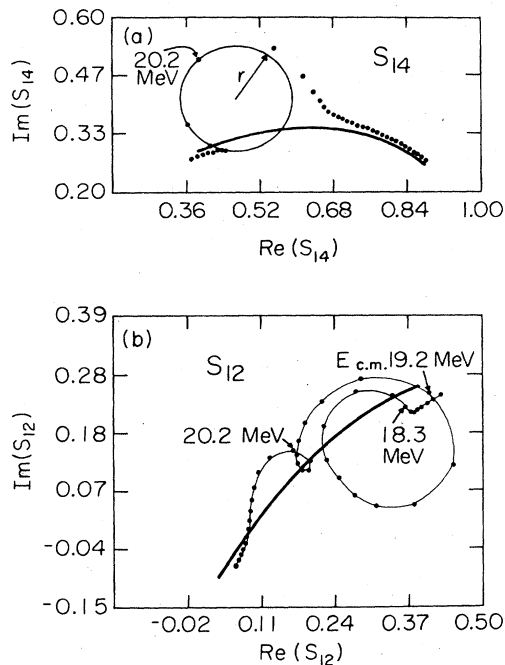


FIG. 8. In (a) the S matrix for the $l=14$ resonance is plotted (points) in the complex plane; the parameters come from Tables III and IV. The background S matrix is the heavy solid curve. The circle is used to obtain the ratio of the elastic width over the total width ($\Gamma_{el}/\Gamma=r$) described in the text. In (b) the S matrix for three $l=12$ resonances included in a three-level formulation is plotted (points). The background S matrix is represented by the heavy solid curve. The light curve through the points is to guide the eye.

causes the trajectory of the sum to describe a loop in the complex plane as the energy passes through the resonance energy. If the background is independent of energy, this loop will describe a circle and the radius of the circle, limited by unitarity to be less than one, will be equal to the ratio of the elastic width to the total width. In Fig. 8(a) the calculated $l=14$ background (solid curve) and the background plus single-level S matrix elements (points) are plotted as functions of energy. The resonance loop is open-ended because the background is changing slowly with energy. Extracting the radius of the loop from Fig. 8(a), one obtains $\Gamma_{el}/\Gamma=0.12$. As expected, this is also the value calculated from the resonance parameters for $l=14$ given in Table III.

In Fig. 8(b) the S matrix calculated for $l=12$ using the parameters of Table III and IV is plotted. Note that there are only two loops rather than three. Apparently, the off diagonal terms in the three-level calculation are strong enough to destroy the loop that would otherwise result from the diagonal term in the level matrix for the 18.3 MeV resonance. The radius of each loop in Fig. 8(b) was measured to obtain a quantity analogous to the ratio of the elastic width to the total width that one would obtain from a Breit-Wigner single level analysis.

The analysis of Fig. 8 results in a ratio of elastic to total widths for the $l=12$ resonances at 19.2 and 20.2 MeV of approximately 0.12 and 0.04, respectively, and a ratio of 0.12 for the $l=14$ resonance at 20.2 MeV. The first (zero phase) solution of Ledoux *et al.* resulted in ratios Γ_{el}/Γ equal to 0.20 and 0.16 for $l=12$ resonances at 19.3 and 20.3 MeV, respectively. The second (large phase) solution of Ledoux *et al.* resulted in ratios $\Gamma_{el}/\Gamma=0.18$ for an $l=12$ resonance at 19.3 MeV and $\Gamma_{el}/\Gamma=0.14$ for an $l=14$ resonance at 20.3 MeV.

In the paper of Ledoux *et al.*,⁷ for the second solution, a total width of 300 keV is reported for the $l=14$ resonance at 20.3 MeV. We obtain (see Table III) a total width of 250 keV for our 14^+ resonance at 20.2 MeV. So there is quite good agreement between our results and the second solution of Ledoux *et al.* regarding both the strength and width of the 14^+ resonance near 20.2 MeV.

SUMMARY

Analysis of excitation function data between the energies of 17.5 and 21.5 MeV leads us to conclude that the peaks observed near 18.4 and 19.3 MeV in the total reaction cross section are due to single resonances with spin 12^+ at the energies of 18.3 and 19.2 MeV, confirming the findings of Ledoux *et al.* Analysis of data at the zeros of P_{12} and P_{14} shows that the third structure near 20.3 MeV is not due to a single resonance as reported by Ledoux *et al.*,⁷ but is due to at least two resonances near 20.2 MeV, one with spin 14^+ . The other we have assigned spin 12^+ . The fact that our optical model plus resonance calculation, with three $l=12$ levels at 18.3, 19.2, and 20.2 MeV and one $l=14$ level at 20.2 MeV, does not give a good fit to the data over the entire energy range indicates that the elastic scattering at this energy is influenced by more than the four levels which we have included in our calculations. Considerable effort was devoted to finding single additional levels which would resolve the discrepancy between the data and calculation at the lower and upper extremes of the excitation function data; however, without success.

Resonance strengths have been extracted for the $l=12$ resonances at 19.2 and 20.2 MeV and the $l=14$ resonance at 20.2 MeV from an analysis of the plotted S matrix curve in the complex plane. The strengths for the $l=12$ resonance at 19.2 and the $l=14$ resonance at 20.2 MeV are in good agreement with the second solution of Ledoux *et al.*⁷ No comparison is possible for the $l=12$ resonance at 18.3 MeV since the effects of the interference terms in the three-level formula of this work overpower the diagonal term for the 18.3 MeV resonance.

ACKNOWLEDGMENTS

We would like to acknowledge the assistance of S. J. Padalino in taking the data and to thank R. J. Philpott for many useful discussions about resonance theory. This work was supported in part by the National Science Foundation.

- ¹D. A. Bromley, J. A. Keuhner, and E. Almqvist, *Phys. Rev. Lett.* **4**, 365 (1960).
- ²W. Reilly, R. Wieland, A. Gobbi, M. W. Sachs, and D. A. Bromley, *Nuovo Cimento* **13A**, 897 (1973).
- ³W. Reilly, R. Wieland, A. Gobbi, M. W. Sachs, J. Maher, R. H. Siemssen, D. Mingay, and D. A. Bromley, *Nuovo Cimento* **13A**, 913 (1973).
- ⁴S. K. Korotky, K. A. Erb, S. J. Willet, and D. A. Bromley, *Phys. Rev. C* **20**, 1014 (1979).
- ⁵H. Emling, R. Nowotny, D. Pelte, and G. Schreider, *Nucl. Phys. A* **211**, 600 (1973).
- ⁶D. Shapira, R. G. Stokstad, and D. A. Bromley, *Phys. Rev. C* **10**, 1063 (1974).
- ⁷R. J. Ledoux, M. J. Bechara, C. E. Ordonez, H. A. Al-Juwair, and E. R. Cosman, *Phys. Rev. C* **27**, 1103 (1983).
- ⁸S. Y. Lee, H. W. Wilschut, and R. J. Ledoux, *Phys. Rev. C* **25**, 2844 (1982).
- ⁹R. G. Stokstad, R. M. Wieland, G. R. Satchler, C. B. Fulmer, D. C. Hensley, S. Raman, L. D. Richertsen, A. H. Snell, and P. H. Stelson, *Phys. Rev. C* **20**, 655 (1979).
- ¹⁰R. M. Wieland, R. G. Stokstad, G. R. Satchler, and L. D. Rickertsen, *Phys. Rev. Lett.* **37**, 1458 (1976).
- ¹¹J. J. Kolata, R. M. Freeman, F. Hass, B. Heusch, and A. Gallmann, *Phys. Rev. C* **21**, 579 (1980).
- ¹²E. R. Cosman, R. J. Ledoux, and A. J. Lazzarini, *Phys. Rev. C* **21**, 2111 (1980).
- ¹³L. I. Schiff, *Quantum Mechanics* (McGraw-Hill, New York, 1949).
- ¹⁴A. M. Lane and R. G. Thomas, *Rev. Mod. Phys.* **30**, 257 (1958).
- ¹⁵D. Robson and A. M. Lane, *Phys. Rev.* **161**, 982 (1967).
- ¹⁶W. J. Thompson, J. L. Adams, and D. Robson, *Phys. Rev.* **173**, 975 (1968).
- ¹⁷R. A. Chatwin, J. S. Eck, D. Robson, and A. Richter, *Phys. Rev. C* **1**, 1795 (1970).
- ¹⁸E. R. Cosman, T. M. Cormier, K. Van Bibber, A. Sperduto, G. Young, J. Erskine, L. R. Greenwood, and O. Hansen, *Phys. Rev. Lett.* **35**, 265 (1975).
- ¹⁹K. Van Bibber, E. R. Cosman, A. Sperduto, T. M. Cormier, T. N. Chin, and O. Hansen, *Phys. Rev. Lett.* **32**, 687 (1974).
- ²⁰T. M. Cormier, J. Applegate, G. M. Berkowitz, P. Braun-Munzinger, P. M. Cormier, J. W. Harris, C. M. Jachcinski, L. L. Lee, Jr., J. Barrette, and H. E. Wegner, *Phys. Rev. Lett.* **38**, 940 (1977); T. M. Cormier, C. M. Jachcinski, G. M. Berkowitz, P. Braun-Munzinger, P. M. Cormier, M. Gai, J. W. Harris, J. Barrette, and H. E. Wegner, *Phys. Rev. Lett.* **40**, 924 (1978).
- ²¹G. Kekelis and J. D. Fox, *Phys. Rev. C* **10**, 2613 (1974).
- ²²L. R. Greenwood, R. E. Segel, K. Raghunathan, M. A. Lee, H. T. Fortune, and J. R. Erskine, *Phys. Rev. C* **12**, 156 (1975).
- ²³N. R. Fletcher, J. D. Fox, G. J. KeKelis, G. R. Morgan, and G. A. Norton, *Phys. Rev. C* **13**, 1173 (1978); D. R. James and N. R. Fletcher, *ibid.* **17**, 2248 (1978).
- ²⁴P. Sperr, D. Evers, K. Rudolph, W. Assmann, E. Spindler, P. Konrad, and G. Denhofer, *Phys. Lett.* **49B**, 345 (1974).
- ²⁵R. J. Ledoux, C. E. Ordonez, M. J. Bechara, H. A. Al-Juwair, G. Lavelle, and E. R. Cosman, *Phys. Rev. C* **30**, 866 (1984).
- ²⁶K. A. Eberhard, E. Mathiak, J. Stettmeir, W. Trombik, A. Weidinger, L. N. Wustefeld, and K. G. Bernhardt, *Phys. Lett.* **56B**, 445 (1975); K. A. Eberhard and K. G. Bernhardt, *Phys. Rev. C* **13**, 440 (1976).
- ²⁷H. T. Fortune, T. H. Braid, R. E. Segel, and K. Raghunathan, *Phys. Lett.* **63B**, 403 (1976).
- ²⁸H. T. Fortune, S. C. Headley, L. R. Medsker, T. H. Braid, R. E. Segel, and K. Raghunathan, *Phys. Rev. C* **14**, 1271 (1976).
- ²⁹H. T. Fortune, L. R. Greenwood, R. E. Segel, and J. R. Erskine, *Phys. Rev. C* **15**, 439 (1977).
- ³⁰G. R. Satchler and W. G. Love, *Phys. Rep.* **55**, 183 (1979); J. Cook, *Comput. Phys. Commun.* **25**, 125 (1982).